2020 IEEE/RSJ International Conference on Intelligent Robots and Systems (IROS)
October 25-29, 2020, Las Vegas, NV, USA (Virtual)

Contact Force Estimation and Regulation of a Position-controlled Floating Base System without Joint Torque Information

Guoteng Zhang[1], *Member, IEEE*, Shugen Ma[2], *Fellow, IEEE*, and Yibin Li[3]

***Abstract*— A floating base system is inevitably to contact the environment while it is moving. This paper explores the contact force estimation and regulation algorithm for a position-controlled floating base system without joint torque information. First, the joint space dynamic model of the system is presented and transformed into the contact space. Then, the inverse dynamics method is employed to estimate the contact forces. After that, a proportional-integral (PI) regulator is designed to drive the contact forces to track the desired values. Finally, the feasibility of this algorithm is demonstrated on a simulated bipedal platform.**

I. Introduction

Legged robots locomote themselves forward by contacting the environments and "manipulating" the environments backward. They are often termed as floating base systems owing to their under-actuated dynamics w.r.t. (with respect to) the inertial reference frames. Compared to the fixed base manipulators, the control of floating base systems is more complex because they are subject to varying contact forces with the environment. Therefore, reading and regulating the contact forces are necessary for generating a high-performance dynamic legged motion.

A traditional method for acquiring contact force feedback is to equip force sensors at the contact locations. However, adding force sensors will greatly increase the cost and complexity of the system. Therefore, some researchers have been trying to indirectly estimate the contact forces acting on the floating base systems instead of directly measuring them. Mistry et. al. [1] pointed out that the contact constraint forces to a floating base system can be estimated iteratively with the joint torques and the dynamic model. Camurri et al. [2] computed the grounding reacting forces (GRFs) to the feet of the quadruped robot HyQ with the feedback of joint positions, velocities, and torques. The tactile sensor network together with the other body sensors on the humanoid robot iCub enabled it to estimate the external forces [3] [4] [5]. Fakoorian et al. [6] designed a continuous-time extended Kalman filter and a continuous-time unscented Kalman filter to estimate the GRFs acted on the feet of prosthetic legs. Benallegue et al. [7] [8] estimated the foot reaction forces of a humanoid robot using the inertial measurement unit (IMU) and the elastic materials under the robot feet. Bledt et al. [9] presented a discrete-time extension of the generalized-momentum disturbance observer to conduct proprioceptive foot force estimates for the MIT Cheetah 3 robot.

If the feedback of contact forces is available, the contact forces can be regulated by constructing a contact force close loop and actuating the robot accordingly. References [10] [11] show examples for this idea. Moreover, some contact force distribution algorithms for floating base systems have been addressed in the literature, from both the controlling and planning points of view. Examples include the motion planner by Hauser et al. [12], the contact space control framework by Khatib et al. [13] [14], the task space inverse dynamics control method by Prete et al. [15], the contact force distribution optimization method by Li et al. [16] [17] and the orthogonal decomposition of inverse dynamics by Righetti et al. [18].

The aforementioned methods had demonstrated their effectiveness in estimating or regulating contact forces to the floating base systems. However, in these researches, the robotic platforms were force-controlled, or at least the joint torque information is known. To the best of the authors' knowledge, there is no prior study on the contact force estimation and regulation of a position-controlled floating base system without joint torque or contact force feedback. Here the "position-control" means that the robot has very stiff actuation and we can only control its joint positions or velocities instead of the forces/torques. Besides, the joint force/torque feedback is not available. The robot is composed of rigid links and there are no elastic elements on the robot.

In this work, we propose an algorithm to estimate and regulate the contact forces of a position-controlled floating base system. This algorithm works even if the joint torque information is unknown. The main results of this paper are listed as follow:

- We have deduced the contact space dynamic model of a floating base system. This model gives us the relationship between the contact forces and the robot base accelerations.
- We have proposed a method to estimate the overall contact forces using only the system's kinematic feedback. The robot joint acceleration or robot base position feedback is not needed for this method.
- We have proposed a solution to dynamically regulate the overall contact forces by iteratively programming

This work was supported by the project of Robotics Innovation Based on Advanced Materials under Ritsumeikan Global Innovation Research Organization (R-GIRO), and the China Postdoctoral Science Foundation (2019M662359).

[1]Guoteng Zhang is now with the School of Control Science and Engineering, Shandong University, Jinan, China. This work was partially conducted while he was working at the Ritsumeikan Global Innovation Research Organization, Ritsumeikan University, Shiga, Japan. (email: zhanggt@sdu.edu.cn)

[2]Shugen Ma is with the Department of Robotics, Ritsumeikan University, Shiga, Japan. (email: shugen@se.ritsumei.ac.jp)

[3]Yibin Li is with the School of Control Science and Engineering, Shandong University, Jinan, China. (email: liyb@sdu.edu.cn)

the joint accelerations.
- The feasibility of our algorithm is evaluated through the bipedal jogging test.

The rest of this paper is organized as follows. Section II gives the motivation for this work. Section III presents the system dynamic modeling in the joint space and contact space. In Section IV, we propose the contact force estimation and regulation algorithm. Experimental evaluations are described in Section V. Finally, Section VI gives the conclusion of this paper.

II. Motivation

A combination of motors and high-ratio gears is widely used as actuators for legged robots. Examples of these robots include Asimo [19], TITAN [20] and Little Dog [21]. The high-ratio gears enabled these robots to generate large joint torques and perform high-gain position control. The robots demonstrated quasi-statically stable walking and sometimes showed a little bit dynamic performance with the help of delicately programmed motion trajectories. However, it is difficult for them to intuitively read or control their joint torques using the motor currents, as loss of motor torque and output power occurs during their transmission by the gears. The joints of robots become stiff and nonbackdrivable due to the high-ratio gears [22]. Many researchers have spent plenty of attention on the modeling of high reduction gear transmissions to get better torque estimation on each joint, such as the works described in [23] [24] [25]. But in dynamic locomotion of legged robot, velocity and acceleration of joint motion vary in a quite wide range, the friction of gear transmission will become very complicated while the robot interacting with the environment.

In the past few years, legged robots such as the quadruped MIT Cheetah [26] [27] [28] and biped ATRIAS [29], have embraced high-torque motors with low-ratio or no transmissions. In these robots, joint torque can be approximated as torque constant multiplied by the current observed from the motor. However, the gear reduction is too low to provide enough load capacity for these quasi-direct-drive systems.

To read or control the joint torques of the robots whose joints are actuated by motors with high-ratio reduction gears, or other stiff actuators such as hydraulic cylinders, extra force sensing elements are often equipped on the actuators. For example, torque sensors were equipped on the output gears of the motor actuated HAA joints in the HyQ quadruped robot, and load cells were mounted on the ends of cylinder rods that actuated the HFE and KFE joints in HyQ [30]. Elastic components are also frequently utilized as force sensing/regulating elements, known as Series Elastic Actuators (SEAs) [31]. StarlETH [32] and its successor ANYmal [33] provide examples for this case. But, the extra force sensing elements will increase the size, weight, and cost of the robot joints.

To summarize, although many of today's legged platforms are force-controlled, their actuating systems have to be elaborately designed and manufactured. Compare to the force-control mode, the position-control mode is easier, lower-cost, and more direct for legged robots with stiff actuators. Therefore, in this paper, we will find a way to estimate and regulate the contact forces of a floating-based legged robot without knowing joint torque information. We hope it could help to avoid the pitfalls of relying on delicate force sensing techniques for controlling highly dynamic legged robots.

III. Floating Base Dynamics

In this section, we model the system dynamics in its joint space and contact space. This gives us the relationship between the contact forces and the robot motion.

A. System Description

Denote the system configuration as

$$\boldsymbol{q} = \begin{bmatrix} \boldsymbol{p}^T & \boldsymbol{\theta}_{\mathrm{S}}^T & \boldsymbol{\theta}_{\mathrm{C}}^T \end{bmatrix}^T \tag{1}$$

where $\boldsymbol{p} \in \mathbb{R}^{n\times 1}$ represents the n degrees of freedom (DOFs) of the robot base, including the position and orientation of the robot base. $n \leqslant 6$. $\boldsymbol{\theta}_{\mathrm{S}} \in \mathbb{R}^{a\times 1}$ is the joint configuration of the rigid-body robot's swing limbs with a joints. $\boldsymbol{\theta}_{\mathrm{C}} \in \mathbb{R}^{b\times 1}$ is the joint configuration of the rigid-body robot's limbs that are in contact with the environment.

The differential kinematics equation of the robot is written as

$$\underbrace{\begin{bmatrix} \dot{\boldsymbol{p}}_{n\times 1} \\ \dot{\boldsymbol{e}}_{\mathrm{S}\,k\times 1} \\ \dot{\boldsymbol{e}}_{\mathrm{C}\,l\times 1} \end{bmatrix}}_{\dot{\boldsymbol{e}}} = \underbrace{\left[\begin{array}{c|c|c} \boldsymbol{I}_{n\times n} & \boldsymbol{0}_{n\times a} & \boldsymbol{0}_{n\times b} \\ \hline \boldsymbol{J}_{p\mathrm{S}\,k\times n} & \boldsymbol{J}_{\theta\mathrm{S}\,k\times a} & \boldsymbol{0}_{k\times b} \\ \hline \boldsymbol{J}_{p\mathrm{C}\,l\times n} & \boldsymbol{0}_{l\times a} & \boldsymbol{J}_{\theta\mathrm{C}\,l\times b} \end{array}\right]}_{\boldsymbol{J}} \underbrace{\begin{bmatrix} \dot{\boldsymbol{p}}_{n\times 1} \\ \dot{\boldsymbol{\theta}}_{\mathrm{S}\,a\times 1} \\ \dot{\boldsymbol{\theta}}_{\mathrm{C}\,b\times 1} \end{bmatrix}}_{\dot{\boldsymbol{q}}} \tag{2}$$

where $\boldsymbol{e}_{\mathrm{S}} \in \mathbb{R}^{k\times 1}$ represents the positions and orientations of the swing limbs' distal ends. $\boldsymbol{e}_{\mathrm{C}} \in \mathbb{R}^{l\times 1}$ represents the positions and orientations of the contact locations between the robot and the environment. $\boldsymbol{J}$ is the Jacobian Matrix and we make it full row rank hence all the parameters in $\boldsymbol{e}$ are linearly independent. For systems with its $\boldsymbol{J}$ being not full row rank, one can easily find a reduced number of independent parameters in $\boldsymbol{e}$, for example by using the SVD decomposition of $\boldsymbol{J}$ [18].

In this paper, we assume that the contact forces are sufficient to hold the contacts steady and no motion is observed at these contact locations with respect to the inertial frame. Hence we have

$$\dot{\boldsymbol{e}}_{\mathrm{C}} = \ddot{\boldsymbol{e}}_{\mathrm{C}} = \boldsymbol{0} \tag{3}$$

B. Joint Space Dynamic Model

When the robot is in contact with the environment, its joint space dynamics with respect to an inertial frame can be written as

$$\boldsymbol{M}\ddot{\boldsymbol{q}} + \boldsymbol{C}\dot{\boldsymbol{q}} + \boldsymbol{g} = \boldsymbol{S}_{\boldsymbol{\tau}}\boldsymbol{\tau} + \boldsymbol{J}^T\boldsymbol{S}_{\boldsymbol{f}}\boldsymbol{f}_{\mathrm{C}} \tag{4}$$

with variables defined as

- $\boldsymbol{M} \in \mathbb{R}^{(n+a+b)\times(n+a+b)}$: the floating base inertia matrix.
- $\boldsymbol{C} \in \mathbb{R}^{(n+a+b)\times(n+a+b)}$: the floating base Coriolis / centripetal matrix.
- $\boldsymbol{g} \in \mathbb{R}^{(n+a+b)\times 1}$: the floating base gravity vector.

- $\boldsymbol{S_\tau} = \begin{bmatrix}\boldsymbol{0}_{(a+b)\times n} & \boldsymbol{I}_{(a+b)\times(a+b)}\end{bmatrix}^T$: the actuated joint selection matrix.
- $\boldsymbol{\tau} \in \mathbb{R}^{(a+b)\times 1}$: the vector of actuated joint torques.
- $\boldsymbol{S_f} = \begin{bmatrix}\boldsymbol{0}_{l\times(n+k)} & \boldsymbol{I}_{l\times l}\end{bmatrix}^T$: the contact force selection matrix.
- $\boldsymbol{f}_\mathrm{C} \in \mathbb{R}^{l\times 1}$: the vector of l contact forces at $\boldsymbol{e}_\mathrm{C}$.

C. Contact Space Dynamic Model

Define the matrix

$$\boldsymbol{V} = \boldsymbol{I} - \boldsymbol{J}^T(\boldsymbol{J}\boldsymbol{M}^{-1}\boldsymbol{J}^T)\boldsymbol{J}\boldsymbol{M}^{-1} := \begin{bmatrix}\boldsymbol{V_1} \\ \hline \boldsymbol{V_2}\end{bmatrix} \begin{matrix}{\scriptstyle (n+a+b)\times n} \\ \hline {\scriptstyle (n+a+b)\times(a+b)}\end{matrix} \tag{5}$$

Then, according to [34], we can express the joint torques in terms of the equivalent forces $\boldsymbol{\gamma}$ at the robot base and contact locations using the following equation:

$$\boldsymbol{S\tau} = \boldsymbol{J}^T\boldsymbol{\gamma} + \boldsymbol{V\tau_0}, \quad \boldsymbol{\tau_0} \in \mathsf{Null}(\boldsymbol{V_1}) \tag{6}$$

where $\boldsymbol{\tau_0}$ is the vector of arbitrary torques within the null space of $\boldsymbol{V_1}$. It is worth noting that $\boldsymbol{f}_\mathrm{C}$ in (4) represents the contribution of the forces due to contacts with the environment, and $\boldsymbol{\gamma}$ in (6) expresses the contribution of the forces due to joint actuation [34].

Putting (6) into (4), we get

$$\boldsymbol{M\ddot{q}} + \boldsymbol{C\dot{q}} + \boldsymbol{g} = \boldsymbol{J}^T\boldsymbol{\gamma} + \boldsymbol{V\tau_0} + \boldsymbol{J}^T\boldsymbol{S_f}\boldsymbol{f}_\mathrm{C} \tag{7}$$

Based on (2), the system's second-order differential kinematics equation can be written as

$$\ddot{\boldsymbol{e}} = \boldsymbol{J\ddot{q}} + \dot{\boldsymbol{J}}\dot{\boldsymbol{q}} \tag{8}$$

Premultiplying (7) by $\boldsymbol{J}\boldsymbol{M}^{-1}$ and combining (8), we can get

$$\ddot{\boldsymbol{e}} + (\boldsymbol{J}\boldsymbol{M}^{-1}\boldsymbol{C} - \dot{\boldsymbol{J}})\dot{\boldsymbol{q}} + \boldsymbol{J}\boldsymbol{M}^{-1}\boldsymbol{g} = \boldsymbol{J}\boldsymbol{M}^{-1}\boldsymbol{J}^T\boldsymbol{\gamma} + \boldsymbol{J}\boldsymbol{M}^{-1}\boldsymbol{J}^T\boldsymbol{S_f}\boldsymbol{f}_\mathrm{C} \tag{9}$$

Since $\boldsymbol{J}$ is full row rank, $\boldsymbol{J}\boldsymbol{M}^{-1}\boldsymbol{J}^T$ should be invertible and we can get $\boldsymbol{\gamma}$ as

$$\boldsymbol{\gamma} = \left(\boldsymbol{J}\boldsymbol{M}^{-1}\boldsymbol{J}^T\right)^{-1}\left(\ddot{\boldsymbol{e}} + (\boldsymbol{J}\boldsymbol{M}^{-1}\boldsymbol{C} - \dot{\boldsymbol{J}})\dot{\boldsymbol{q}} + \boldsymbol{J}\boldsymbol{M}^{-1}\boldsymbol{g}\right) - \boldsymbol{S_f}\boldsymbol{f}_\mathrm{C} \tag{10}$$

Putting (10) into (6), we obtain

$$\bar{\boldsymbol{M}}\ddot{\boldsymbol{e}} + \bar{\boldsymbol{C}}\dot{\boldsymbol{q}} + \bar{\boldsymbol{g}} = \boldsymbol{S\tau} - \boldsymbol{V\tau_0} + \boldsymbol{J}^T\boldsymbol{S_f}\boldsymbol{f}_\mathrm{C} \tag{11}$$

where

$$\bar{\boldsymbol{M}} = \boldsymbol{J}^T\left(\boldsymbol{J}\boldsymbol{M}^{-1}\boldsymbol{J}^T\right)^{-1},\ \bar{\boldsymbol{C}} = \bar{\boldsymbol{M}}(\boldsymbol{J}\boldsymbol{M}^{-1}\boldsymbol{C} - \dot{\boldsymbol{J}}),\ \bar{\boldsymbol{g}} = \bar{\boldsymbol{M}}\boldsymbol{J}\boldsymbol{M}^{-1}\boldsymbol{g}$$

Considering (1)(2)(3)(5)(6), (11) can be rewritten as

$$\begin{bmatrix}\bar{\boldsymbol{M}}_{11} & \bar{\boldsymbol{M}}_{12} & \bar{\boldsymbol{M}}_{13} \\ {\scriptstyle n\times n} & {\scriptstyle n\times k} & {\scriptstyle n\times l} \\ \bar{\boldsymbol{M}}_{21} & \bar{\boldsymbol{M}}_{22} & \bar{\boldsymbol{M}}_{23} \\ {\scriptstyle a\times n} & {\scriptstyle a\times k} & {\scriptstyle a\times l} \\ \bar{\boldsymbol{M}}_{31} & \bar{\boldsymbol{M}}_{32} & \bar{\boldsymbol{M}}_{33} \\ {\scriptstyle b\times n} & {\scriptstyle b\times k} & {\scriptstyle b\times l}\end{bmatrix}\begin{bmatrix}\ddot{\boldsymbol{p}} \\ {\scriptstyle n\times 1} \\ \ddot{\boldsymbol{e}}_\mathrm{S} \\ {\scriptstyle k\times 1} \\ \boldsymbol{0} \\ {\scriptstyle l\times 1}\end{bmatrix} + \begin{bmatrix}\bar{\boldsymbol{C}}_{11} & \bar{\boldsymbol{C}}_{12} & \bar{\boldsymbol{C}}_{13} \\ {\scriptstyle n\times n} & {\scriptstyle n\times a} & {\scriptstyle n\times b} \\ \bar{\boldsymbol{C}}_{21} & \bar{\boldsymbol{C}}_{22} & \bar{\boldsymbol{C}}_{23} \\ {\scriptstyle a\times n} & {\scriptstyle a\times a} & {\scriptstyle a\times b} \\ \bar{\boldsymbol{C}}_{31} & \bar{\boldsymbol{C}}_{32} & \bar{\boldsymbol{C}}_{33} \\ {\scriptstyle b\times n} & {\scriptstyle b\times a} & {\scriptstyle b\times b}\end{bmatrix}\begin{bmatrix}\dot{\boldsymbol{p}} \\ {\scriptstyle n\times 1} \\ \dot{\boldsymbol{\theta}}_\mathrm{S} \\ {\scriptstyle a\times 1} \\ \dot{\boldsymbol{\theta}}_\mathrm{C} \\ {\scriptstyle b\times 1}\end{bmatrix} + \begin{bmatrix}\bar{\boldsymbol{g}}_1 \\ {\scriptstyle n\times 1} \\ \bar{\boldsymbol{g}}_2 \\ {\scriptstyle a\times 1} \\ \bar{\boldsymbol{g}}_3 \\ {\scriptstyle b\times 1}\end{bmatrix}$$

$$= \begin{bmatrix}\boldsymbol{0} \\ {\scriptstyle n\times 1} \\ \boldsymbol{\tau}\end{bmatrix} - \begin{bmatrix}\boldsymbol{0} \\ {\scriptstyle n\times 1} \\ \boldsymbol{V_2\tau_0}\end{bmatrix} + \begin{bmatrix}\boldsymbol{I} & \boldsymbol{J}_{p_\mathrm{S}}^T & \boldsymbol{J}_{p_\mathrm{C}}^T \\ {\scriptstyle n\times n} & {\scriptstyle n\times k} & {\scriptstyle n\times l} \\ \boldsymbol{0} & \boldsymbol{J}_{\theta_\mathrm{S}}^T & \boldsymbol{0} \\ {\scriptstyle a\times n} & {\scriptstyle a\times k} & {\scriptstyle a\times l} \\ \boldsymbol{0} & \boldsymbol{0} & \boldsymbol{J}_{\theta_\mathrm{C}}^T \\ {\scriptstyle b\times n} & {\scriptstyle b\times k} & {\scriptstyle b\times l}\end{bmatrix}\begin{bmatrix}\boldsymbol{0} \\ {\scriptstyle (n+k)\times 1} \\ \boldsymbol{f}_\mathrm{C}\end{bmatrix} \tag{12}$$

No joint torque element exists in the upper n rows of (12). We can then determine the principle between the contact forces and robot motions as the following equation:

$$\bar{\boldsymbol{M}}_{11}\ddot{\boldsymbol{p}} + \bar{\boldsymbol{M}}_{12}\ddot{\boldsymbol{e}}_\mathrm{S} + \bar{\boldsymbol{C}}_{11}\dot{\boldsymbol{p}} + \bar{\boldsymbol{C}}_{12}\dot{\boldsymbol{\theta}}_\mathrm{S} + \bar{\boldsymbol{C}}_{13}\dot{\boldsymbol{\theta}}_\mathrm{C} + \bar{\boldsymbol{g}}_1 = \boldsymbol{J}_{p_\mathrm{C}}^T\boldsymbol{f}_\mathrm{C} \tag{13}$$

Considering $\ddot{\boldsymbol{e}}_\mathrm{S} = \boldsymbol{J}_{p_\mathrm{S}}\ddot{\boldsymbol{p}} + \boldsymbol{J}_{\theta_\mathrm{S}}\ddot{\boldsymbol{\theta}}_\mathrm{S} + \dot{\boldsymbol{J}}_{p_\mathrm{S}}\dot{\boldsymbol{p}} + \dot{\boldsymbol{J}}_{\theta_\mathrm{S}}\dot{\boldsymbol{\theta}}_\mathrm{S}$, (13) can be converted to

$$\boldsymbol{\Lambda}\ddot{\boldsymbol{p}} + \boldsymbol{\Phi}\ddot{\boldsymbol{\theta}}_\mathrm{S} + \boldsymbol{\Omega}\dot{\boldsymbol{q}} + \boldsymbol{\eta} = \boldsymbol{J}_{p_\mathrm{C}}^T\boldsymbol{f}_\mathrm{C} \tag{14}$$

where

$$\boldsymbol{\Lambda} = \bar{\boldsymbol{M}}_{11} + \bar{\boldsymbol{M}}_{12}\boldsymbol{J}_{p_\mathrm{S}},\quad \boldsymbol{\Phi} = \bar{\boldsymbol{M}}_{12}\boldsymbol{J}_{\theta_\mathrm{S}},\quad \boldsymbol{\eta} = \bar{\boldsymbol{g}}_1,$$
$$\boldsymbol{\Omega} = \left[\begin{array}{c|c|c} \bar{\boldsymbol{C}}_{11} + \bar{\boldsymbol{M}}_{12}\dot{\boldsymbol{J}}_{p_\mathrm{S}} & \bar{\boldsymbol{C}}_{12} + \bar{\boldsymbol{M}}_{12}\dot{\boldsymbol{J}}_{\theta_\mathrm{S}} & \bar{\boldsymbol{C}}_{13}\end{array}\right]$$

In (14), we have eliminated the joint torque vector and obtained the relationship between contact forces and robot base accelerations. In this paper, we refer to it as the system's contact space dynamic model.

IV. Contact Force Estimation and Regulation

This section firstly gives the definition of the overall contact forces. Then, the contact force estimating method is deduced and its necessary sensing devices are listed. Finally, we present the contact force regulator and explain how it works.

A. Overall Contact Forces

The $\boldsymbol{J}_{p_\mathrm{C}}^T\boldsymbol{f}_\mathrm{C}$ in (14) represents the virtual forces acted on the robot base that are generated by the contact forces $\boldsymbol{f}_\mathrm{C}$. Only if $\boldsymbol{J}_{p_\mathrm{C}}$ is full row rank will we will be able to calculate $\boldsymbol{f}_\mathrm{C}$ from (14). For systems with its $\boldsymbol{J}_{p_\mathrm{C}}$ being not full row rank, one can easily find a reduced number of independent contact forces w.r.t. $\boldsymbol{J}_{p_\mathrm{C}}$. For example, two round tips contacting with the floor can be equivalently represented as a vector with 5 parameters: 3-dimensional force parameters and 2-dimensional moment parameters, while three tips contacting with the environment can be described using the 3-dimensional force parameters together with 3-dimensional moment parameters. We denote this procedure as

$$\boldsymbol{f}_\mathrm{G} = \boldsymbol{H}\boldsymbol{f}_\mathrm{C} \tag{15}$$

and

$$\boldsymbol{f}_\mathrm{C} = \boldsymbol{H}^T(\boldsymbol{H}\boldsymbol{H}^T)^{-1}\boldsymbol{f}_\mathrm{G} + \mathsf{Null}(\boldsymbol{J}_{p_\mathrm{C}}^T) \tag{16}$$

where $\boldsymbol{f}_\mathrm{G} \in \mathbb{R}^{g\times 1}$ is the vector of independent contact forces for $\boldsymbol{J}_{p_\mathrm{C}}^T$. $\boldsymbol{H} \in \mathbb{R}^{l\times g}$ stands for the transform matrix. $g \leqslant l$ and $g \leqslant n$.

$\boldsymbol{f}_\mathrm{G}$ physically stands for the interactive forces and moments between the environment and the overall robot. In this paper, we name $\boldsymbol{f}_\mathrm{G}$ as the *overall contact forces*. In particular, if $\boldsymbol{J}_{p_\mathrm{C}}$ is full row rank, $\boldsymbol{f}_\mathrm{G} = \boldsymbol{f}_\mathrm{C}$.

Putting (16) into (14), we obtain the dynamics for overall contact forces:

$$\boldsymbol{\Lambda}\ddot{\boldsymbol{p}} + \boldsymbol{\Phi}\ddot{\boldsymbol{\theta}}_\mathrm{S} + \boldsymbol{\Omega}\dot{\boldsymbol{q}} + \boldsymbol{\eta} = \boldsymbol{J}_\mathrm{G}^T\boldsymbol{f}_\mathrm{G} \tag{17}$$

where

$$\boldsymbol{J}_\mathrm{G} = (\boldsymbol{H}\boldsymbol{H}^T)^{-1}\boldsymbol{H}\boldsymbol{J}_{p_\mathrm{C}} \tag{18}$$

B. Contact Force Estimation

Premultiplying (17) by $(\boldsymbol{J}_{\mathrm{G}}\boldsymbol{J}_{\mathrm{G}}^{T})^{-1}\boldsymbol{J}_{\mathrm{G}}$, we get

$$\boldsymbol{f}_{\mathrm{G}} = (\boldsymbol{J}_{\mathrm{G}}\boldsymbol{J}_{\mathrm{G}}^{T})^{-1}\boldsymbol{J}_{\mathrm{G}}\left(\boldsymbol{\Lambda}\ddot{\boldsymbol{p}} + \boldsymbol{\Phi}\ddot{\boldsymbol{\theta}}_{\mathrm{S}} + \boldsymbol{\Omega}\dot{\boldsymbol{q}} + \boldsymbol{\eta}\right) \tag{19}$$

The joint acceleration $\ddot{\boldsymbol{\theta}}_{\mathrm{S}}$ is difficult to obtain in a practical system. To solve this problem, we check the differential equation governing the dynamics of a single joint of multi-DOF robot:

$$\tau_{\mathrm{a}} - \tau_{\mathrm{d}} = I_m\ddot{\theta} \tag{20}$$

where τ_{a} is the torque generated by the joint actuator, τ_{d} is the total disturbing torque acted on the joint axis. I_m is the total moment of inertia of the payload. θ is the joint angle.

In a high-stiff position-controlled legged robot, the actuating joint torque can be considered as a large gain w.r.t. the joint position error:

$$\tau_{\mathrm{a}} = k_{\mathrm{a}}({}^{\mathrm{d}}\theta - \theta) \tag{21}$$

where k_{a} is the gain of the position closed loop, and ${}^{\mathrm{d}}\theta$ is the desired joint position.

Combining (20)(21) and denoting s as the Laplace variable, we can get

$$\ddot{\theta} = \frac{k_{\mathrm{a}}}{k_{\mathrm{a}} + s^2 I_m}{}^{\mathrm{d}}\ddot{\theta} - \frac{s^2}{k_{\mathrm{a}} + s^2 I_m}\tau_{\mathrm{d}} \tag{22}$$

While the robot limb is swing freely without interacting with the environment, the equivalent payload and disturbance to the joint will not perform great changes. Hence the $s^2 I_m$ and $s^2\tau_{\mathrm{d}}$ should have limited scales. If the joint position feedback gain k_{a} is sufficiently large, (22) becomes

$$\ddot{\theta} \approx {}^{\mathrm{d}}\ddot{\theta} \tag{23}$$

which implies that by a large position gain the robot can suppress both the disturbing torque and the uncertain disturbance in payload. Therefore, for a position-controlled swing limb with stiff actuation, we can take the joint accelerations as approximately equal to their reference values, i.e.:

$$\ddot{\boldsymbol{\theta}}_{\mathrm{S}} \approx {}^{\mathrm{d}}\ddot{\boldsymbol{\theta}}_{\mathrm{S}} \tag{24}$$

Then the estimated value of the overall contact force $\boldsymbol{f}_{\mathrm{G}}$ can be obtained through the following equation:

$$\widehat{\boldsymbol{f}}_{\mathrm{G}} = (\widetilde{\boldsymbol{J}}_{\mathrm{G}}\widetilde{\boldsymbol{J}}_{\mathrm{G}}^{T})^{-1}\widetilde{\boldsymbol{J}}_{\mathrm{G}}\left(\widetilde{\boldsymbol{\Lambda}}\ddot{\widetilde{\boldsymbol{p}}} + \widetilde{\boldsymbol{\Omega}}\dot{\widetilde{\boldsymbol{q}}} + \widetilde{\boldsymbol{\eta}} + \widetilde{\boldsymbol{\Phi}}\ddot{\boldsymbol{\theta}}_{\mathrm{Sref}}\right) \tag{25}$$

where the hat and tilde symbols indicate the estimated and measured values, respectively. Similarly hereinafter.

Now we will demonstrate that, in a position-controlled floating base system, it is practical to acquire the measured values on the right side of (25). We further illustrate the system configuration $\boldsymbol{q}$ as

$$\boldsymbol{q} = \begin{bmatrix}\boldsymbol{p}^T & \boldsymbol{\theta}_{\mathrm{S}}^T & \boldsymbol{\theta}_{\mathrm{C}}^T\end{bmatrix}^T = \begin{bmatrix}\boldsymbol{x}^T & \boldsymbol{\varphi}^T & \boldsymbol{\theta}_{\mathrm{S}}^T & \boldsymbol{\theta}_{\mathrm{C}}^T\end{bmatrix} \tag{26}$$

where $\boldsymbol{x}$ and $\boldsymbol{\varphi}$ represent the position vector and orientating angle vector of the robot base, respectively. We can see that the right side of (25) can be calculated based on $\widetilde{\boldsymbol{\theta}}_{\mathrm{S}}$, $\widetilde{\boldsymbol{\theta}}_{\mathrm{C}}$, $\dot{\widetilde{\boldsymbol{\theta}}}_{\mathrm{S}}$, $\dot{\widetilde{\boldsymbol{\theta}}}_{\mathrm{C}}$, $\dot{\widetilde{\boldsymbol{x}}}$, $\ddot{\widetilde{\boldsymbol{x}}}$, $\dot{\widetilde{\boldsymbol{\varphi}}}$, $\widetilde{\boldsymbol{\varphi}}$, and $\ddot{\widetilde{\boldsymbol{\varphi}}}$. In a position-controlled robotic system, these requisite feedback values can be obtained through the following methods:

- $\widetilde{\boldsymbol{\theta}}_{\mathrm{S}}$ and $\widetilde{\boldsymbol{\theta}}_{\mathrm{C}}$ can be measured using the joint position sensors.
- $\dot{\widetilde{\boldsymbol{\theta}}}_{\mathrm{S}}$ and $\dot{\widetilde{\boldsymbol{\theta}}}_{\mathrm{C}}$ can be obtained through numerical differentiating $\widetilde{\boldsymbol{\theta}}_{\mathrm{S}}$ and $\widetilde{\boldsymbol{\theta}}_{\mathrm{C}}$.
- $\dot{\widetilde{\boldsymbol{\varphi}}}$ and $\widetilde{\boldsymbol{\varphi}}$ can be measured using the gyroscope mounted on the robot base.
- $\ddot{\widetilde{\boldsymbol{\varphi}}}$ can be obtained through numerical differentiating $\dot{\widetilde{\boldsymbol{\varphi}}}$, or measured using an angular accelerometer.
- $\ddot{\widetilde{\boldsymbol{x}}}$ can be measured using the accelerometer mounted on the robot base.
- $\dot{\widetilde{\boldsymbol{x}}}$ can be inferred through leg odometry or state estimation techniques [35].

Note that the robot base position $\widetilde{\boldsymbol{x}}$ is not required in solving (25). Please check the appendix for explanation.

C. Contact Force Regulation

In this part, we will propose an iterative method to regulate the overall contact forces of the floating base system. Denote

$$\boldsymbol{\Pi} = (\boldsymbol{J}_{\mathrm{G}}\boldsymbol{\Lambda}^{-1}\boldsymbol{J}_{\mathrm{G}}^{T})^{-1}(\boldsymbol{H}\boldsymbol{H}^{T})^{-1}\boldsymbol{H}$$
$$\boldsymbol{\Upsilon} = (\boldsymbol{J}_{\mathrm{G}}\boldsymbol{\Lambda}^{-1}\boldsymbol{J}_{\mathrm{G}}^{T})^{-1}\boldsymbol{J}_{\mathrm{G}}\boldsymbol{\Lambda}^{-1}$$

If the current overall system contact force is $\widehat{\boldsymbol{f}}_{\mathrm{G}(t)}$ ($\widehat{\boldsymbol{f}}_{\mathrm{G}(t)}$ can be obtained via (25)), and the desired contact force at the next control cycle is noted as ${}^{\mathrm{d}}\boldsymbol{f}_{\mathrm{G}(t+\Delta t)}$, the requisite joint acceleration of the robot's contact limbs ${}^{\mathrm{d}}\ddot{\boldsymbol{\theta}}_{\mathrm{C}(t+\Delta t)}$ should be:

$$\begin{aligned}{}^{\mathrm{d}}\ddot{\boldsymbol{\theta}}_{\mathrm{C}(t+\Delta t)} = &-\left(\widetilde{\boldsymbol{\Pi}}_{(t)}\boldsymbol{J}_{\theta\mathrm{C}(t)}\right)^{T}\left(\left(\widetilde{\boldsymbol{\Pi}}_{(t)}\boldsymbol{J}_{\theta\mathrm{C}(t)}\right)\left(\widetilde{\boldsymbol{\Pi}}_{(t)}\boldsymbol{J}_{\theta\mathrm{C}(t)}\right)^{T}\right)^{-1}\\ &\bullet\Big({}^{\mathrm{d}}\boldsymbol{f}_{\mathrm{G}(t+\Delta t)} + \boldsymbol{k}_{\mathrm{I}}\sum_{0}^{t/\Delta t+1}\left({}^{\mathrm{d}}\boldsymbol{f}_{\mathrm{G}(t+\Delta t)} - \widehat{\boldsymbol{f}}_{\mathrm{G}(t)}\right)\Delta t\\ &-\widetilde{\boldsymbol{\Upsilon}}_{(t)}\left(\widetilde{\boldsymbol{\Phi}}_{(t)}{}^{\mathrm{d}}\ddot{\boldsymbol{\theta}}_{\mathrm{S}(t+\Delta t)} + \widetilde{\boldsymbol{\eta}}_{(t)}\right)\Big)\end{aligned} \tag{27}$$

where $\boldsymbol{k}_{\mathrm{I}}$ is the vector for integral parameters. Δt represents the period of the system's control cycle. Note that in (27) we assume a full-ranked $\boldsymbol{\Lambda}$. For the case that $\boldsymbol{\Lambda}$ not being full rank, one may consider to employ the generalized inverse in (27). Validity of the regulator in (27) is demonstrated below.

If $\boldsymbol{\Lambda}$ is invertible, premultiplying (17) by $\boldsymbol{\Upsilon}$ results in the following equation:

$$\boldsymbol{f}_{\mathrm{G}} - \boldsymbol{\Upsilon}\left(\boldsymbol{\Omega}\dot{\boldsymbol{q}} + \boldsymbol{\eta} + \boldsymbol{\Phi}\ddot{\boldsymbol{\theta}}_{\mathrm{S}}\right) = (\boldsymbol{J}_{\mathrm{G}}\boldsymbol{\Lambda}^{-1}\boldsymbol{J}_{\mathrm{G}}^{T})^{-1}\boldsymbol{J}_{\mathrm{G}}\ddot{\boldsymbol{p}} \tag{28}$$

Combining (2)(3)(18) yields

$$\boldsymbol{J}_{\mathrm{G}}\ddot{\boldsymbol{p}} = -(\boldsymbol{H}\boldsymbol{H}^{T})^{-1}\boldsymbol{H}\left(\dot{\boldsymbol{J}}_{p\mathrm{C}}\dot{\boldsymbol{p}} + \boldsymbol{J}_{\theta\mathrm{C}}\ddot{\boldsymbol{\theta}}_{\mathrm{C}} + \dot{\boldsymbol{J}}_{\theta\mathrm{C}}\dot{\boldsymbol{\theta}}_{\mathrm{C}}\right) \tag{29}$$

Putting (29) into (28), we can get

$$\boldsymbol{f}_{\mathrm{G}} + \boldsymbol{\Pi}\left(\dot{\boldsymbol{J}}_{p\mathrm{C}}\dot{\boldsymbol{p}} + \dot{\boldsymbol{J}}_{\theta\mathrm{C}}\dot{\boldsymbol{\theta}}_{\mathrm{C}}\right) - \boldsymbol{\Upsilon}\left(\boldsymbol{\Omega}\dot{\boldsymbol{q}} + \boldsymbol{\eta} + \boldsymbol{\Phi}\ddot{\boldsymbol{\theta}}_{\mathrm{S}}\right) = -\boldsymbol{\Pi}\boldsymbol{J}_{\theta\mathrm{C}}\ddot{\boldsymbol{\theta}}_{\mathrm{C}} \tag{30}$$

Plugging our regulator (27) into (30), we can get the system dynamics for $(t+\Delta t)$ to be

$$\begin{aligned}&\left({}^{\mathrm{d}}\boldsymbol{f}_{\mathrm{G}(t+\Delta t)}-\boldsymbol{f}_{\mathrm{G}(t+\Delta t)}\right)+\boldsymbol{k}_{\mathrm{I}}\sum_{0}^{t/\Delta t+1}\left({}^{\mathrm{d}}\boldsymbol{f}_{\mathrm{G}(t+\Delta t)}-\widehat{\boldsymbol{f}}_{\mathrm{G}(t)}\right)\Delta t\\ =&\boldsymbol{\Pi}_{(t+\Delta t)}\left(\boldsymbol{J}_{p\mathrm{C}(t+\Delta t)}\dot{\boldsymbol{p}}_{(t+\Delta t)}+\dot{\boldsymbol{J}}_{\theta\mathrm{C}(t+\Delta t)}\dot{\boldsymbol{\theta}}_{\mathrm{C}(t+\Delta t)}\right)\\ &-\boldsymbol{\Upsilon}_{(t+\Delta t)}\left(\boldsymbol{\Omega}_{(t+\Delta t)}\dot{\boldsymbol{q}}_{(t+\Delta t)}+\boldsymbol{\eta}_{(t+\Delta t)}+\boldsymbol{\Phi}_{(t+\Delta t)}\ddot{\boldsymbol{\theta}}_{\mathrm{S}(t+\Delta t)}\right)\\ &+\widetilde{\boldsymbol{\Upsilon}}_{(t)}\left(\widetilde{\boldsymbol{\Phi}}_{(t)}{}^{\mathrm{d}}\ddot{\boldsymbol{\theta}}_{\mathrm{S}(t+\Delta t)}+\widetilde{\boldsymbol{\eta}}_{(t)}\right)\end{aligned}\tag{31}$$

If the system control period Δt is sufficiently short, the system configuration and the contact forces will rarely change between two contiguous control cycles. Hence we can have

$$\begin{cases}\boldsymbol{f}_{\mathrm{G}(t+\Delta t)}\approx\widehat{\boldsymbol{f}}_{\mathrm{G}(t)}, & \boldsymbol{\Upsilon}_{(t+\Delta t)}\approx\widetilde{\boldsymbol{\Upsilon}}_{(t)},\\ \boldsymbol{\Phi}_{(t+\Delta t)}\approx\widetilde{\boldsymbol{\Phi}}_{(t)}, & \boldsymbol{\eta}_{(t+\Delta t)})\approx\widetilde{\boldsymbol{\eta}}_{(t)},\\ \ddot{\boldsymbol{\theta}}_{\mathrm{S}(t+\Delta t)}\approx{}^{\mathrm{d}}\ddot{\boldsymbol{\theta}}_{\mathrm{S}(t+\Delta t)}.\end{cases}\tag{32}$$

Combining (31)(32), we derive:

$$\left({}^{\mathrm{d}}\boldsymbol{f}_{\mathrm{G}(t+\Delta t)}-\boldsymbol{f}_{\mathrm{G}(t+\Delta t)}\right)+\boldsymbol{k}_{\mathrm{I}}\sum_{0}^{t/\Delta t+1}\left({}^{\mathrm{d}}\boldsymbol{f}_{\mathrm{G}(t+\Delta t)}-\boldsymbol{f}_{\mathrm{G}(t+\Delta t)}\right)\Delta t=\boldsymbol{\varepsilon}\tag{33}$$

with $\boldsymbol{\varepsilon}$ being

$$\begin{aligned}\boldsymbol{\varepsilon}=\boldsymbol{\Pi}_{(t+\Delta t)}&\left(\boldsymbol{J}_{p\mathrm{C}(t+\Delta t)}\dot{\boldsymbol{p}}_{(t+\Delta t)}+\dot{\boldsymbol{J}}_{\theta\mathrm{C}(t+\Delta t)}\dot{\boldsymbol{\theta}}_{\mathrm{C}(t+\Delta t)}\right)\\ &-\boldsymbol{\Upsilon}_{(t+\Delta t)}\boldsymbol{\Omega}_{(t+\Delta t)}\dot{\boldsymbol{q}}_{(t+\Delta t)}+\boldsymbol{\varepsilon}_{\mathbf{0}}\end{aligned}\tag{34}$$

where $\boldsymbol{\varepsilon}_{\mathbf{0}}$ represents the vector of errors caused by the approximation in (32).

The left side of (33) is a PI controller about the errors between desired contact forces and actual contact forces. This PI controller will eliminate the errors and make the actual values track the desired values. Note that in (27), the velocity items are not compensated because it is difficult to predict the system velocities at $(t+\Delta t)$ while the joints are conducting accelerating motions.

In a position-controlled platform, it may be difficult to directly control the joint accelerations. Instead, we can set the desired joint position using the following principle:

$${}^{\mathrm{d}}\boldsymbol{\theta}_{\mathrm{C}(t+\Delta t)}=\widetilde{\boldsymbol{\theta}}_{\mathrm{C}(t)}+\boldsymbol{k}_{\theta}\left(\widetilde{\dot{\boldsymbol{\theta}}}_{\mathrm{C}(t)}\Delta t+\frac{1}{2}{}^{\mathrm{d}}\ddot{\boldsymbol{\theta}}_{\mathrm{C}(t+\Delta t)}\Delta t^{2}\right)\tag{35}$$

where $\boldsymbol{k}_{\theta}$ is a diagonal matrix for manually tuned gains.

V. Evaluations

In this section, we show the feasibility of the contact force estimation and regulation algorithm on a simulated bipedal platform that performed the jogging motion. Video for the test is available through the attached file of this paper.

A. Bipedal Platform

In order to test the performance of the force estimating and regulating algorithm for high dynamic motions, a bipedal platform was built in the robot simulator *Webots R2019b revision 1*. Fig. 1 shows a photo of the simulation model with illustrations of its key parameters. The robotic platform consisted of a body and two identical legs. The body was

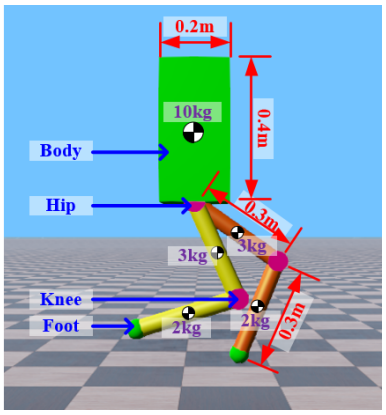

Fig. 1. The bipedal robotic platform built in the simulator.

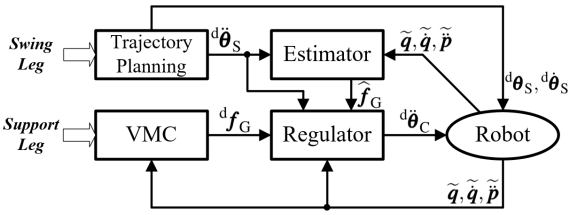

Fig. 2. Block diagram of the bipedal robot controller. VMC: virtual model controller.

restricted to move within its sagittal plane with a fixed attitude angle, i.e., it had a horizontal DOF and a vertical DOF. Each leg had two position-controlled revolute joints: the hip joint and the knee joint, enabling the foot to move within the two-dimensional plane. Hence we have $n=a=b=k=l=2$. There was a contact switch at each robot foot to tell whether the foot touched the ground or not. The control cycle frequency in the simulator was 1000Hz.

In order to detect the actual values of the contact forces, we embedded a force sensor at each robot foot. The detected forces were only used for data comparison, not used in the robot control.

B. Robot Controller

The jogging motion entailed a continuous series of hops from one leg to the other. Each leg of the bipedal robot experienced the support and swing phases. Duty factor for the support phase was set to 0.3. In the support phase, the leg was virtualized to a spring-damper element, which is known as the virtual model control. The virtual spring was compressed and then performed a thrust motion to the ground. During the "thrust" period we injected extra energy to the virtual spring to compensate for the energy loss in each hopping motion. The virtualized foot force was converted to desired joint accelerations by the contact force regulator and estimator. In the flight phase, we just simply designed the foot swing trajectory and then actuated the joints through inverse kinematics. Fig. 2 gives the control block diagram for the jogging motion.

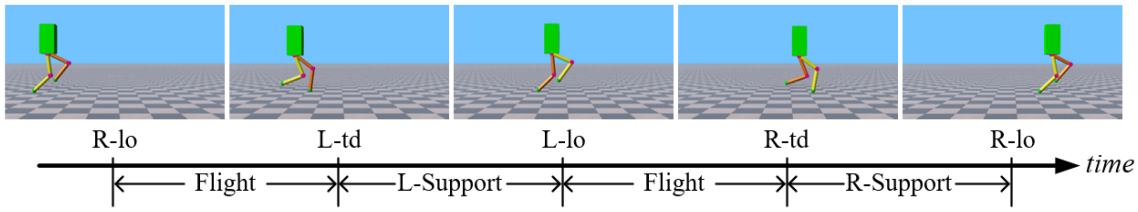

Fig. 3. Snapshots of the biped jogging simulation with illustrations of the states. L: left foot; R: right foot; lo: liftoff; td: touchdown.

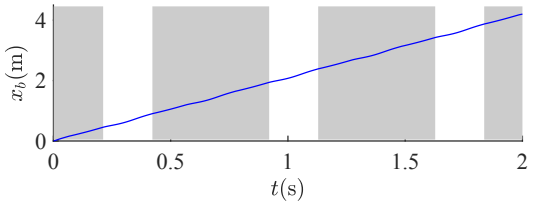

(a) Horizontal positon of the robot body.

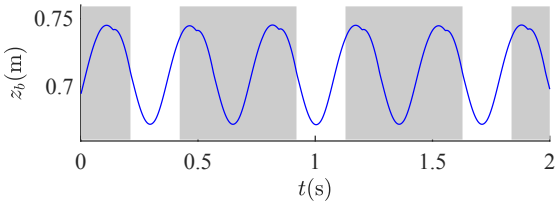

(b) Vertical positon of the robot body.

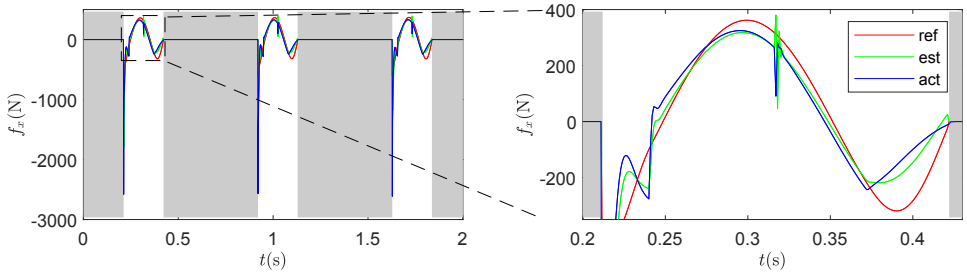

(c) The horizontal contact force to the robot's left foot. The red curve represents the reference value. The green curve represents the estimated value. The blue curve represents the actual value monitored via the simulator. The right figure is an enlarged drawing of the contents in the dotted box of the left figure.

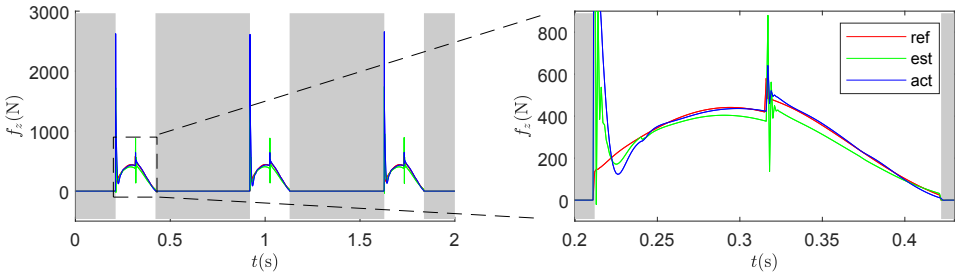

(d) The vertical contact force to the robot's left foot. The red curve represents the reference value. The green curve represents the estimated value. The blue curve represents the actual value monitored via the simulator. The right figure is an enlarged drawing of the contents in the dotted box of the left figure.

Fig. 4. Time plots of the robot body position and left foot's contact force during the simulation. The grey areas indicate that the left foot is in swing phases and the white areas indicate the left foot's support phases.

C. Results

Our controller successfully actuated the bipedal platform to jog with various horizontal speeds. Fig. 3 displays some snapshots of the jogging motion. Fig. 4 shows the performance of our controller. We can see the trajectory of the robot body successfully mimicked that of a spring-load system. The estimated contact force values were close to the actual ones. At the moments that the foot hit the ground, the estimated and actual contact forces exhibited large impulses. This phenomenon was consistent with those of the force-controlled hopping platforms described in [36] [37]. After the short impulses, the estimated and actual contact forces could track the desired values.

In this test, errors in the force estimation were probably due to the shift of contact points. In the simulation, the robot foot was a 60mm diameter ball instead of an idealized pinpoint. Therefore, even if there was no slippage between the foot and the ground, the contact point between them would still change slightly during the motion, which was not consistent with (3).

The error between desired values and actual values of the contact forces was mainly caused by two reasons. The first one is the estimation errors, as we used the estimated values instead of the actual values in our contact force regulator. The

second reason could be found in the PI controller in (33), since we were not able to set the proportional parameters and hence the regulating gains were limited, which restricted the system performance in high dynamic motions.

VI. Conclusion

This paper gives an approach to estimate and regulate the contact forces of a position-controlled floating base system based on the contact space dynamic model. The basic idea within this approach is that the interaction between the robot and the environment will influence the motion of robot base. By measuring the robot joint configuration and base orientation, the overall forces at the fixed contact locations can be estimated. By controlling the robot joint accelerations based on the system status feedback, these contact forces can be regulated. Feedback of robot joint accelerations and robot base position is not needed in this approach.

The major contribution of this paper is that it provides a solution to dynamically control the interactive forces between the legged robots and the environment without force controlling or measuring techniques. We have demonstrated the feasibility of our algorithm with evaluations on a simulated bipedal robot. It enabled the biped to perform jogging motion, with acceptable contact force estimating and tracking performances.

The framework reported in this paper requires that the robotic system can provide accurate kinematic feedback and exhibit good position/velocity tracking abilities. In future work, we will test its performance on physical platforms and check its robustness to actuating errors and feedback noises.

Appendix

This appendix shows the fact that the robot base position vector $\widetilde{\boldsymbol{x}}$ does not exist in (25) or (27). The proof is quite complex. Here we only describe the basic idea within the proving process due to lacking space.

Consider the most general case that $n=6$ and denote the robot base position as $\boldsymbol{x}=[x_b\ y_b\ z_b]^T$. Then according to (26), the system configuration $\boldsymbol{q}$ can be written as

$$\boldsymbol{q}=\left[x_b\ y_b\ z_b\ \boldsymbol{\varphi}^T\ \boldsymbol{\theta}_{\mathrm{S}}^T\ \boldsymbol{\theta}_{\mathrm{C}}^T\right]^T \tag{36}$$

One can find that, for an arbitrary point on the robot, its direct kinematics function with respect to the inertial frame can be expressed by the homogeneous transformation matrix

$$\boldsymbol{T}(\boldsymbol{q})=\left[\begin{array}{ccc|c} & \boldsymbol{R}(\boldsymbol{\varphi},\boldsymbol{\theta}_{\mathrm{S}},\boldsymbol{\theta}_{\mathrm{C}}) & & \begin{array}{c}x_b+p_x(\boldsymbol{\varphi},\boldsymbol{\theta}_{\mathrm{S}},\boldsymbol{\theta}_{\mathrm{C}})\\ y_b+p_y(\boldsymbol{\varphi},\boldsymbol{\theta}_{\mathrm{S}},\boldsymbol{\theta}_{\mathrm{C}})\\ z_b+p_z(\boldsymbol{\varphi},\boldsymbol{\theta}_{\mathrm{S}},\boldsymbol{\theta}_{\mathrm{C}})\end{array} \\ \hline 0 & 0 & 0 & 1 \end{array}\right] \tag{37}$$

Therefore, the corresponding Jacobian matrix does not contain x_b, y_b, or z_b.

Then, following (37), we can find that, in the *Lagrangian* of the robotic system, the elements that contain x_b, y_b, or z_b are irrelevant with other variables. That is, the system *Lagrangian* can be written as

$$L=k_x x_b+k_y y_b+k_z z_b+L(\boldsymbol{\varphi},\boldsymbol{\theta}_{\mathrm{S}},\boldsymbol{\theta}_{\mathrm{C}},\dot{\boldsymbol{\varphi}},\dot{\boldsymbol{\theta}}_{\mathrm{S}},\dot{\boldsymbol{\theta}}_{\mathrm{C}},\dot{x}_b,\dot{y}_b,\dot{z}_b) \tag{38}$$

where k_x, k_y and k_z are constant coefficients.

According to Lagrangian Formulation, the system dynamics (4) can be obtained by

$$\frac{\mathrm{d}}{\mathrm{d}t}\frac{\partial L}{\partial \dot{q}_i}-\frac{\partial L}{\partial q_i}=\xi_i \qquad i=1,2,...,n+a+b \tag{39}$$

where ξ_i is the generalized force associated with the generalized coordinate q_i.

Putting (36)(38) into (39), we can find that x_b, y_b and z_b vanished and hence (4) does not contain the robot base position parameters in $\boldsymbol{x}$. Since (25) and (27) are deduced based on (4) and the system Jacobian, we can prove that the feedback of robot base position $\widetilde{\boldsymbol{x}}$ is not needed in our contact force estimation and regulation algorithm.

References

[1] M. Mistry, J. Buchli, and S. Schaal, "Inverse dynamics control of floating base systems using orthogonal decomposition," in *2010 IEEE International Conference on Robotics and Automation*. Citeseer, 2010, pp. 3406–3412.

[2] M. Camurri, M. Fallon, S. Bazeille, A. Radulescu, V. Barasuol, D. G. Caldwell, and C. Semini, "Probabilistic contact estimation and impact detection for state estimation of quadruped robots," *IEEE Robotics and Automation Letters*, vol. 2, no. 2, pp. 1023–1030, 2017.

[3] A. Del Prete, L. Natale, F. Nori, and G. Metta, "Contact force estimations using tactile sensors and force/torque sensors," in *Human Robot Interaction*, vol. 2012, 2012, pp. 0–2.

[4] M. Fumagalli, S. Ivaldi, M. Randazzo, L. Natale, G. Metta, G. Sandini, and F. Nori, "Force feedback exploiting tactile and proximal force/torque sensing," *Autonomous Robots*, vol. 33, no. 4, pp. 381–398, 2012.

[5] F. J. A. Chavez, J. Kangro, S. Traversaro, F. Nori, and D. Pucci, "Contact force and joint torque estimation using skin," *IEEE Robotics and Automation Letters*, vol. 3, no. 4, pp. 3900–3907, 2018.

[6] S. Fakoorian, V. Azimi, M. Moosavi, H. Richter, and D. Simon, "Ground reaction force estimation in prosthetic legs with nonlinear kalman filtering methods," *Journal of Dynamic Systems, Measurement, and Control*, vol. 139, no. 11, p. 111004, 2017.

[7] A. Mifsud, M. Benallegue, and F. Lamiraux, "Estimation of contact forces and floating base kinematics of a humanoid robot using only inertial measurement units," in *2015 IEEE/RSJ International Conference on Intelligent Robots and Systems*. IEEE, 2015, pp. 3374–3379.

[8] M. Benallegue and F. Lamiraux, "Estimation and stabilization of humanoid flexibility deformation using only inertial measurement units and contact information," *International Journal of Humanoid Robotics*, vol. 12, no. 03, p. 1550025, 2015.

[9] G. Bledt, P. M. Wensing, S. Ingersoll, and S. Kim, "Contact model fusion for event-based locomotion in unstructured terrains," in *2018 IEEE International Conference on Robotics and Automation (ICRA)*. IEEE, 2018, pp. 1–8.

[10] C. Fu and K. Chen, "Gait synthesis and sensory control of stair climbing for a humanoid robot," *IEEE Transactions on Industrial Electronics*, vol. 55, no. 5, pp. 2111–2120, 2008.

[11] S. Noda, M. Murooka, S. Nozawa, Y. Kakiuchi, K. Okada, and M. Inaba, "Generating whole-body motion keep away from joint torque, contact force, contact moment limitations enabling steep climbing with a real humanoid robot," in *2014 IEEE International Conference on Robotics and Automation*. IEEE, 2014, pp. 1775–1781.

[12] K. Hauser, T. Bretl, J.-C. Latombe, K. Harada, and B. Wilcox, "Motion planning for legged robots on varied terrain," *The International Journal of Robotics Research*, vol. 27, no. 11-12, pp. 1325–1349, 2008.

[13] L. Sentis and O. Khatib, "Control of free-floating humanoid robots through task prioritization," in *2005 IEEE International Conference on Robotics and Automation*. IEEE, 2005, pp. 1718–1723.

[14] J. Park and O. Khatib, "Contact consistent control framework for humanoid robots," in *2006 IEEE International Conference on Robotics and Automation*. IEEE, 2006, pp. 1963–1969.

[15] A. Del Prete, F. Nori, G. Metta, and L. Natale, "Prioritized motion–force control of constrained fully-actuated robots:"task space inverse dynamics"," *Robotics and Autonomous Systems*, vol. 63, pp. 150–157, 2015.

[16] Z. Li, S. S. Ge, and S. Liu, "Contact-force distribution optimization and control for quadruped robots using both gradient and adaptive neural networks," *IEEE transactions on neural networks and learning systems*, vol. 25, no. 8, pp. 1460–1473, 2014.

[17] Z. Li, S. Xiao, S. S. Ge, and H. Su, "Constrained multilegged robot system modeling and fuzzy control with uncertain kinematics and dynamics incorporating foot force optimization," *IEEE Transactions on Systems, Man, and Cybernetics: Systems*, vol. 46, no. 1, pp. 1–15, 2016.

[18] L. Righetti, J. Buchli, M. Mistry, M. Kalakrishnan, and S. Schaal, "Optimal distribution of contact forces with inverse-dynamics control," *The International Journal of Robotics Research*, vol. 32, no. 3, pp. 280–298, 2013.

[19] Y. Sakagami, R. Watanabe, C. Aoyama, S. Matsunaga, N. Higaki, and K. Fujimura, "The intelligent asimo: System overview and integration," in *IEEE/RSJ international conference on intelligent robots and systems*, vol. 3. IEEE, 2002, pp. 2478–2483.

[20] K. Arikawa and S. Hirose, "Development of quadruped walking robot titan-viii," in *Proceedings of the 1996 IEEE/RSJ International Conference on Intelligent Robots and Systems*, vol. 1. IEEE, 1996, pp. 208–214.

[21] M. P. Murphy, A. Saunders, C. Moreira, A. A. Rizzi, and M. Raibert, "The littledog robot," *The International Journal of Robotics Research*, vol. 30, no. 2, pp. 145–149, 2011.

[22] Y. Fujimoto, T. Kominami, and H. Hamada, "Development and analysis of a high thrust force direct-drive linear actuator," *IEEE Transactions on Industrial Electronics*, vol. 56, no. 5, pp. 1383–1392, 2009.

[23] T. D. Tuttle and W. P. Seering, "A nonlinear model of a harmonic drive gear transmission," *IEEE Transactions on Robotics and Automation*, vol. 12, no. 3, pp. 368–374, 1996.

[24] H. Zhang, S. Ahmad, and G. Liu, "Torque estimation technique of robotic joint with harmonic drive transmission," in *2013 IEEE International Conference on Robotics and Automation*. IEEE, 2013, pp. 3034–3039.

[25] Y. Nagamatsu, T. Shirai, H. Suzuki, Y. Kakiuchi, K. Okada, and M. Inaba, "Distributed torque estimation toward low-latency variable stiffness control for gear-driven torque sensorless humanoid," in *2017 IEEE/RSJ International Conference on Intelligent Robots and Systems (IROS)*. IEEE, 2017, pp. 5239–5244.

[26] S. Seok, A. Wang, M. Y. M. Chuah, D. J. Hyun, J. Lee, D. M. Otten, J. H. Lang, and S. Kim, "Design principles for energy-efficient legged locomotion and implementation on the mit cheetah robot," *Ieee/asme transactions on mechatronics*, vol. 20, no. 3, pp. 1117–1129, 2014.

[27] G. Bledt, M. J. Powell, B. Katz, J. Di Carlo, P. M. Wensing, and S. Kim, "Mit cheetah 3: Design and control of a robust, dynamic quadruped robot," in *2018 IEEE/RSJ International Conference on Intelligent Robots and Systems (IROS)*. IEEE, 2018, pp. 2245–2252.

[28] B. Katz, J. Di Carlo, and S. Kim, "Mini cheetah: A platform for pushing the limits of dynamic quadruped control," in *2019 International Conference on Robotics and Automation (ICRA)*. IEEE, 2019, pp. 6295–6301.

[29] C. Hubicki, J. Grimes, M. Jones, D. Renjewski, A. Spröwitz, A. Abate, and J. Hurst, "Atrias: Design and validation of a tether-free 3d-capable spring-mass bipedal robot," *The International Journal of Robotics Research*, vol. 35, no. 12, pp. 1497–1521, 2016.

[30] C. Semini, N. G. Tsagarakis, E. Guglielmino, M. Focchi, F. Cannella, and D. G. Caldwell, "Design of hyq–a hydraulically and electrically actuated quadruped robot," *Proceedings of the Institution of Mechanical Engineers, Part I: Journal of Systems and Control Engineering*, vol. 225, no. 6, pp. 831–849, 2011.

[31] G. A. Pratt and M. M. Williamson, "Series elastic actuators," in *Proceedings 1995 IEEE/RSJ International Conference on Intelligent Robots and Systems. Human Robot Interaction and Cooperative Robots*, vol. 1. IEEE, 1995, pp. 399–406.

[32] M. Hutter, C. Gehring, M. A. Höpflinger, M. Blösch, and R. Siegwart, "Toward combining speed, efficiency, versatility, and robustness in an autonomous quadruped," *IEEE Transactions on Robotics*, vol. 30, no. 6, pp. 1427–1440, 2014.

[33] M. Hutter, C. Gehring, D. Jud, A. Lauber, C. D. Bellicoso, V. Tsounis, J. Hwangbo, K. Bodie, P. Fankhauser, M. Bloesch *et al.*, "Anymal-a highly mobile and dynamic quadrupedal robot," in *2016 IEEE/RSJ International Conference on Intelligent Robots and Systems (IROS)*. IEEE, 2016, pp. 38–44.

[34] B. Siciliano, L. Sciavicco, L. Villani, and G. Oriolo, "Operational space dynamic model," in *Robotics: modelling, planning and control*. Springer Science & Business Media, 2010.

[35] M. Bloesch, M. Hutter, M. A. Hoepflinger, S. Leutenegger, C. Gehring, C. D. Remy, and R. Siegwart, "State estimation for legged robots-consistent fusion of leg kinematics and imu," *Robotics*, vol. 17, pp. 17–24, 2013.

[36] T. Boaventura, J. Buchli, C. Semini, and D. G. Caldwell, "Model-based hydraulic impedance control for dynamic robots," *IEEE Transactions on Robotics*, vol. 31, no. 6, pp. 1324–1336, 2015.

[37] G. Zhang, Z. Jiang, Y. Li, H. Chai, T. Chen, and Y. Li, "Active compliance control of the hydraulic actuated leg prototype," *Assembly Automation*, vol. 37, no. 3, pp. 356–368, 2017.